SF 298 MASTER COPY KEEP THIS COPY FOR REPRODUCTION PURPOSES

REPORT DOCUMENTATION PAGE

Form Approved
OMB NO. 0704-0188

1. AGENCY USE ONLY (Leave blank)	2. REPORT DATE	3. REPORT TYPE AND DATES COVERED
	July 1996	Technical

4. TITLE AND SUBTITLE
Fractal Estimation of Flank Wear in Turning
Part 1 - Theoretical Foundations and Methodology

5. FUNDING NUMBERS
DAAH04-96-1-0082

6. AUTHOR(S)
S. Bukkapatnam. S.R.T. Kumara, A. Lakhtakia

7. PERFORMING ORGANIZATION NAMES(S) AND ADDRESS(ES)
Center for Multivariate Analysis
417 Classroom Building
The Pennsylvania State University
University Park, PA 16802

8. PERFORMING ORGANIZATION REPORT NUMBER

9. SPONSORING / MONITORING AGENCY NAME(S) AND ADDRESS(ES)
U.S. Army Research Office
P.O. Box 12211
Research Triangle Park, NC 27709-2211

10. SPONSORING / MONITORING AGENCY REPORT NUMBER
ARO 35518.3-MA

11. SUPPLEMENTARY NOTES
The views, opinions and/or findings contained in this report are those of the author(s) and should not be construed as an official Department of the Army position, policy or decision, unless so designated by other documentation.

12a. DISTRIBUTION / AVAILABILITY STATEMENT
Approved for public release: distribution unlimited.

12 b. DISTRIBUTION CODE

13. ABSTRACT (Maximum 200 words)

In this two-part paper, a novel scheme of sensor-based on-line cutting tool flank wear estimation, called fractal estimation is developed, implemented and evaluated. This paradigm is unique in the sense that we extract fractal properties of sensor signals. The metric invariants of the sensor signals called *fractal dimensions* are related to the instantaneous flank wear using a recurrent neural network to implement a *fractal estimator*. The performance of the fractal estimator, evaluated using actual experimental data, establishes this scheme as a viable flank wear estimation paradigm. This methodology is general enough to be applied to many classes of estimation problems related to several manufacturing processes.

We have developed the necessary theoretical formalisms and obtained implementation experiences through the research on tool wear monitoring in turning. The feature extraction methods used in this work are vital to the image analysis research and form the foundation for our future work.

In this first part, theoretical foundations leading to the development of the fractal estimator are presented. New schemes of wavelet transform-based signal separation and fractal dimensions based feature extraction are described in detail.

14. SUBJECT TERMS

15. NUMBER IF PAGES
19

16. PRICE CODE

17. SECURITY CLASSIFICATION OR REPORT	18. SECURITY CLASSIFICATION OF THIS PAGE	19. SECURITY CLASSIFICATION OF ABSTRACT	20. LIMITATION OF ABSTRACT
UNCLASSIFIED	UNCLASSIFIED	UNCLASSIFIED	UL

FRACTAL ESTIMATION OF FLANK WEAR IN TURNING PART–1: THEORETICAL FOUNDATIONS AND METHODOLOGY

Satish Bukkapatnam
Graduate Student in Industrial and Manufacturing Engineering

Soundar R. T. Kumara*
Professor of Industrial and Manufacturing Engineering

Akhlesh Lakhtakia
Associate Professor of Engineering Science and Mechanics
The Pennsylvania State University
University Park, PA 16802

Abstract

In this two-part paper, a novel scheme of sensor-based on-line cutting tool flank wear estimation, called fractal estimation is developed, implemented and evaluated. This paradigm is unique in the sense that we extract fractal properties of sensor signals. The metric invariants of the sensor signals called ***fractal dimensions*** are related to the instantaneous flank wear using a recurrent neural network to implement a ***fractal estimator***. The performance of the fractal estimator, evaluated using actual experimental data, establishes this scheme as a viable flank wear estimation paradigm. This methodology is general enough to be applied to many classes of estimation problems related to several manufacturing processes.

We have developed the necessary theoretical formalisms and obtained implementation experiences through the research on tool wear monitoring in turning. The feature extraction methods used in this work are vital to the image analysis research and form the foundation for our future work.

In this first part, theoretical foundations leading to the development of the fractal estimator are presented. New schemes of wavelet transform-based signal separation and fractal dimensions based feature extraction are described in detail.

*Supported under DAA H04-96-1-0082

Contents

1 INTRODUCTION

1.1 On-line quality control

Today's manufacturing systems are constantly striving to produce low-cost high-quality products in a global environment that demands ever-increasing quality, flexibility and production-rates. This is forcing manufacturing systems towards integration at both sub-systems and systems levels, so that quality and production issues can be addressed right from the product conception stage.

Even when the quality and production requirements are considered from the design stage; product and production failures are bound to occur due to the following reasons:

- lack of complete knowledge of the dynamics of the individual manufacturing processes that a particular manufacturing system is comprised of
- Lack of complete knowledge of the dynamics of the whole system comprising of all concurrent engineering activities, and uncertainties arising therefrom; and
- impossibility of contriving exact sub-systems satisfying specified functional and operational requirements.

The occurrence of product failures can be substantially alleviated by resorting to appropriate control schemes. However, current control systems have been predominantly developed to remedy production-related and machine-specific servo-level problems, but do not cater to quality problems (Hardt, 1993; Ulsoy and Koren, 1993). As a result, integrated process and product quality control systems are not well-developed.

Hence, on-line, real-time quality control schemes for manufacturing processes have to be developed to address quality issues. Given the trend towards globalization of markets, it is imperative that such schemes be robust enough so that consistent-quality products are realized. In order to develop an adequate real-time quality control scheme, the manufacturing process needs to be monitored, faults have to be diagnosed, and a real-time control actions need to be enforced *in situ*. We show in Figure 1 such a scheme for the turning process. Integrated *monitoring, diagnosis and control* systems are deemed essential for successful real-time quality control. But, so far, even the individual tasks and sub-tasks pertaining to monitoring, diagnosis and control of a manufacturing process have not been thoroughly researched (Hardt, 1993).

Our overall objective is to initiate a comprehensive discussion of the relevant issues. At the Intelligent Design and Diagnostics Research Laboratory (IDDRL) at Penn State we have been actively involved with research in the foundations of Intelligent Integrated Diagnositcs (IID). IID is a novel paradigm to integrate the process specific concepts of monitoring, diagnosis and control. In this paper, we concentrate on the monitoring part, specifically with regard to the ubiquitous turning process.

1.2 Scope of monitoring

The turning process, for that matter any manufacturing process, is a dynamical system. From a systems perspective, the state of the turning process is an abstract entity lying in some abstract space Ω; therefore it needs to be transformed into an ensemble of measurable quantities. Let $\mathbf{U}$ be the space of state variables $\{u\}$. Each state variable $\{u\}$ is possibly multi-dimensional and comprised by Borel-measurable functions (Stark and Wood, 1994). We need to select a finite number K of state variables $\{u_1\}, \{u_2\}, \ldots, \{u_K\}$ for physical implementation. For instance, we may choose $K = 2$ for the turning process where $\{u_1\} = \{u_1(P,t)\}$ is the instantaneous tool wear at time t along three orthogonal directions at a selected point P lying on the cutting tool surface, and similarly $\{u_2\} = \{u_2(P,t)\}$ is the instantaneous cutting tool deflection vector. A state variable can be a pointwise function or a bulk function.

The state of any process evolves with time, and fewer than K state variables may be adequate to achieve a specific engineering objective. Some or all of the elements of the chosen state variables may

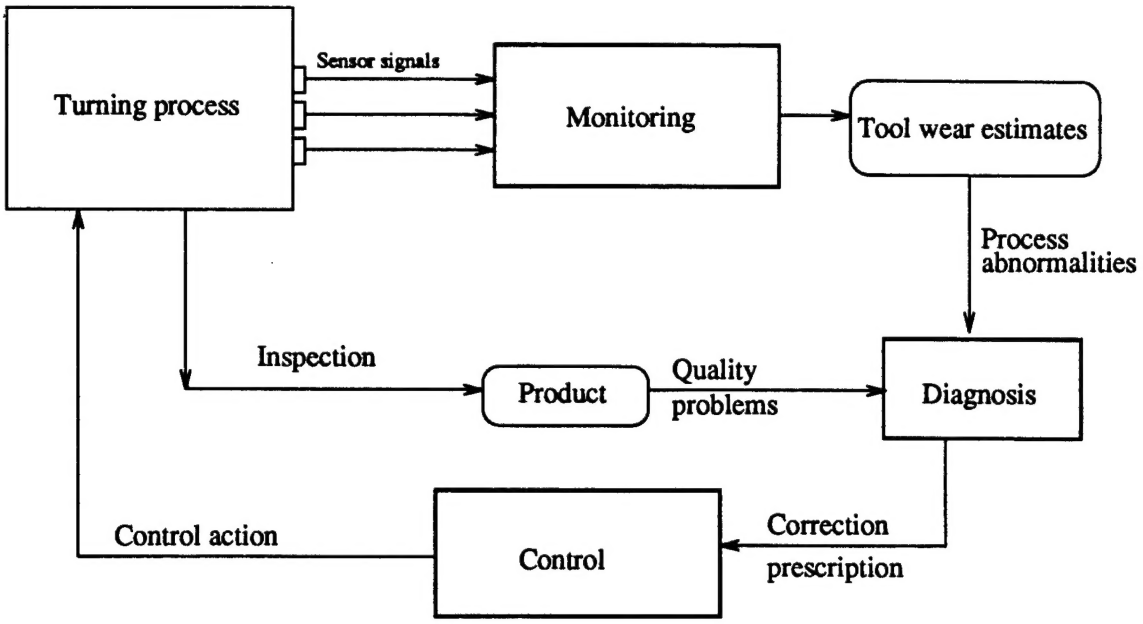

Figure 1: Schematic of the turning process showing the role of monitoring, diagnosis and control systems

be transformed and/or projected into a state vector

$$\mathbf{x} = \mathbf{x}(t) = \begin{bmatrix} x_1 \\ x_2 \\ \vdots \\ x_{d_\mathbf{X}} \end{bmatrix}, \tag{1}$$

The state vectors lie in a $d_\mathbf{X}$-dimensional state space $\mathbf{M}$ of square integrable functions of time alone. The process state is also influenced by the process parameters, represented in a process parameter vector

$$\mathbf{p} = \begin{bmatrix} p_1 \\ p_2 \\ \vdots \\ p_{d_\mathbf{P}} \end{bmatrix} \tag{2}$$

of dimension $d_\mathbf{P}$. For instance, we may define p_1 as the instantaneous cutting speed and p_2 as the instantaneous coolant flow rate. The process dynamics may be mathematically represented by a set of differential/difference equations relating $\mathbf{x}(t)$ and $\mathbf{p}$. However, the exact structure of these equations is in general not known for a real-world process.

Therefore, a model of a particular process dynamics has to be developed from a set of measurements, given by the measurement vector

$$\mathbf{y}(t) = \begin{bmatrix} y_1 \\ y_2 \\ \vdots \\ y_{d_\mathbf{Y}} \end{bmatrix} \tag{3}$$

of dimension $d_\mathbf{Y}$, lying in the measurement space $\mathbf{Y}$. Most elements of $\mathbf{y}(t)$ correspond to some elements of $\mathbf{x}(t)$, or some functions thereof. In general, $d_\mathbf{X} \neq d_\mathbf{Y}$ and measurements are contaminated by noise; however, provided that the noise can be filtered out, we suppose that $\mathbf{x}(t)$ can be completely determined from knowing $\mathbf{y}(t)$. Measurements are usually made at discrete instants t_n of time; therefore we denote

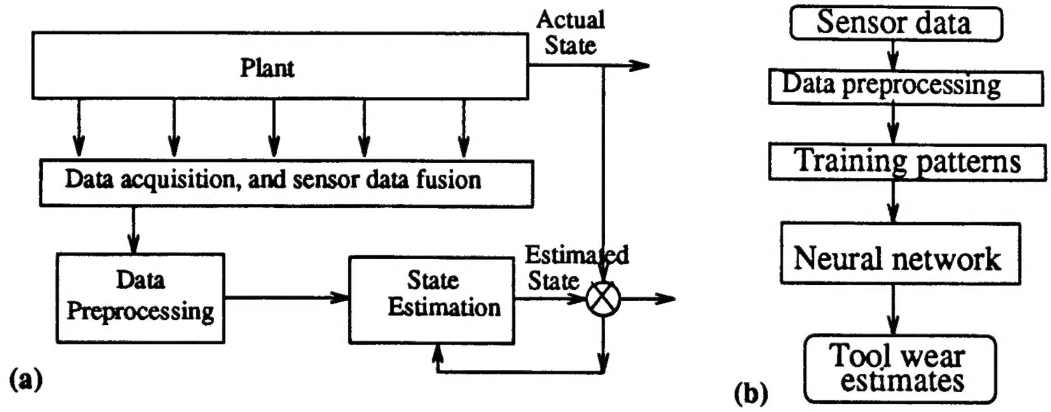

Figure 2: (a) A generalized schema of tool wear estimation, (b) Neural network-based tool wear estimation

$\mathbf{y}(t_n)$ simply as $\mathbf{y}(n)$, where $n, 1 \leq n \leq N$, is the time-index. The ensemble $\mathbf{y}(n), 1 \leq n \leq N$ may be called vector time-series data (TSD).

The performance of the process may be assessed in terms of a scalar functional $z(t)$. This figure of merit is a measurable function of $\mathbf{x}(t)$, and belongs the performance space $\mathbf{G}$.

The state vector $\mathbf{x}$ may be partitioned into a response vector $\mathbf{x}_R$ and a driver vector $\mathbf{x}_D$ such that $\mathbf{x}_R$ is comprised by those elements of $\mathbf{x}$ whose measured values appear as the elements of $\mathbf{y}$. Note that $\mathbf{y}$ completely contains $\mathbf{x}_R$, but may have additional elements that do not lie in $\mathbf{x}_R$. Monitoring involves estimating $\mathbf{x}_D$ from the knowledge of $\mathbf{x}_R$. Whenever the measurements of some state variables of interest are available, such state variables can be directly estimated from the measurements. Monitoring in this case is termed *direct*. When the measurements are not direct determinates of state and/or performance variables (eg., cutting tool wear from the measurements from on-line force, vibration, and acoustic emission sensors), monitoring is termed *indirect*.

Most variables of interest in manufacturing processes, especially the turning process, are inaccessible to direct monitoring. For example, state variables such as product surface characteristics and tool wear cannot be directly measured. Hence, indirect monitoring using on-line sensors is common. This paper describes a paradigm for indirect monitoring of tool wear. The issues concerning tool wear monitoring are described in the following subsection.

1.3 Tool wear monitoring

The prediction and estimation of tool wear in the turning process has been a challenging problem in machine tool monitoring. Owing to the complex mechanical and thermo-chemical phenomena taking place in the cutting zones (Trent, 1991), the material on the surfaces adjoining the cutting edge gets depleted, and the edge becomes blunt. This gradual time-dependent deterioration of cutting tool surface is called tool wear. There are three major types of tool wear: (i) flank wear, (ii) nose wear and (iii) crater wear. Flank wear has the most deleterious effect on the product quality (Boothroyd and Knight, 1989). In particular, the height of the flank wear land h_w has an important bearing on the quality, hence this height is used to represent flank wear.

Due to the inaccessibility of the cutting tool edge for direct on-line measurement, indirect tool wear estimation schemes are usually resorted to. A generalized schema for tool wear state estimation is shown in Figure 2(a). It consists of acquiring the on-line sensor signals, and using the information contained therein for estimating the state of turning dynamics, including cutting tool wear (Kamarthi, 1994). Usually, such schemes are based on—(1) analytical models, (2) observers, or (3) neural networks (NNs) (Kamarthi, 1994). NN-based on-line tool wear estimation is the latest indirect tool wear monitoring method. Sensor fusion techniques coupled with properly designed neural network architectures have resulted in reasonably successful monitoring systems(Kamarthi, 1994; Elanayar and Shin, 1995).

The procedure for designing NN-based tool wear monitoring systems, as shown in Figure 2(b), usually

involves the following steps (Kumara et al., 1994; Kamarthi, 1994):

1. Physical simulation of the actual turning process under controlled experimental conditions, and collection of on-line sensor signals in the form of TSD. The selection and mounting of these sensors depends upon the specific tool wear estimation strategy. The most commonly used sensors for on-line monitoring are force sensors, vibration sensors, acoustic emission sensors, and temperature sensors.
2. Selection of a proper data acquisition strategy (including the choice of sampling rate, sensor specifications, etc.) and proper design of experiments so as to adequately cover the state space of the system under different parameter combinations.
3. Identification of signal contaminants, and design of appropriate signal separation schemes.
4. Selection of feature extraction and data compression methods. The selected features should ideally represent the *invariants* of the system dynamics (synonymously, system invariants), and should constitute a snap-shot of the system dynamics in any sampling interval.
5. Design of an appropriate neural network architecture to relate the features with tool wear, neural network training, and performance testing. Multilayer neural networks, Kohonen's feature maps, and ART networks are normally used.

The NN-based methodology, particularly the signal separation and feature extraction modules, is not fully developed yet. Furthermore, selecting and extracting features is considered an art (Du et al., 1995). This is because, most of the present-day signal separation and feature extraction procedures are based only on the statistical properties of the sensor signals and do not consider the characteristics of the underlying process dynamics.

But the results of our previous research clearly show that turning dynamics exhibits low-dimensional chaos (Bukkapatnam et al., 1995). Hence if we can educe the structural information regarding this chaotic attractor of turning dynamics for signal separation and feature extraction, the resulting monitoring systems will be more robust compared with those developed using only the statistical properties of the signals.

Since turning dynamics is *chaotic*, we employ tools and techniques of *chaos theory* to educe the information from sensor signals for signal separation and feature extraction. In specific, we employ *fractal analysis*—an agglomeration of mathematical techniques to analyze nonlinear TSD for characterizing the specific system through experimentation.

Before describing the specifics of the tools and techniques employed, we give a brief overview of chaos theory and fractal analysis so that the reasoning behind choosing specific tools and techniques becomes more evident. After this brief overview, we present our methodology and describe specific techniques employed therein. Our methodology and reported results, we hope, will spur further research on paradigms based on combining fractal analysis and neural networks for tool wear monitoring and other indirect monitoring problems pertinent to manufacturing processes.

This paper is organized as follows: In Section 2 the significance of chaos theory is presented, in Section 3, a brief introduction to fractal analysis is presented; a description of fractal dimensions is provided in Section 4; and the main motivation for this work is contained in Section 5. Next the overall methodology is given in Section 6. Finally, the two main procedures employed in this paper—signal separation and fractal dimension estimation—are described in Sections 7 and 8, respectively. Implementation details, results and discussion are provided in Part-2 of this paper.

2 CHAOS THEORY

During the past decade, chaos theory has elicited a lot of interest among scientists and researchers. As a result, its ideas are beginning to be applied to many scientific and engineering problems, especially where nonlinear models are relevant (Isham, 1993). The term *chaos* signifies that the evolution of a given dynamical system is so irregular that the system response is highly sensitive to the initial conditions. Initially small differences between two system trajectories grow exponentially in time, thus impairing

long-term predictability. In this section, we provide a concise mathematical treatment of some relevant aspects of chaos theory.

Any system that produces continuous-time response may be modeled by a set of differential equations of the form

$$\frac{d\mathbf{x}(t)}{dt} = F(\mathbf{x}(t)), \tag{4}$$

$F(\cdot)$ is a generally nonlinear *vector field.* The solution to (4) results in a trajectory

$$\mathbf{x}(t) = f(\mathbf{x}(0), t), \tag{5}$$

where $f : \mathbf{M} \mapsto \mathbf{M}$ represents the *flow* that determines the evolution of $\mathbf{x}(t)$ for a particular initial condition $\mathbf{x}(0)$.

If $\mathbf{T} \subset \mathbf{M}$ is *compact*[1] such that $f[\mathbf{T}] = \mathbf{T}$,[2] then $\mathbf{T}$ is said to be invariant under flow f. If volume elements[3] in the state space contract as the system evolves, the system is said to be *dissipative.*[4] If $\mathbf{A} \subset \mathbf{M}$ is a compact set and $\mathcal{U}$ is the largest open set that asymptotically contracts to $\mathbf{A} \subset \mathcal{U}$, then $\mathbf{A}$ is called an *attracting set* and $\mathcal{U}$ is called the *basin of attraction* of $\mathbf{A}$. An attracting set may be reduced into certain distinct portions, some of which may not be attracting. All disjoint subsets $\mathbf{A}_1, \mathbf{A}_2, \mathbf{A}_3, \ldots$ of $\mathbf{A}$ that are attracting are called *attractors*, while $\mathbf{A} - (\bigcup_j \mathbf{A}_j)$ is non-attracting.

In dissipative systems, even though the overall volume of a volume element contract, there can be some directions in which the linear dimension of the volume element actually expands. However, as the attractors are usually bounded, the flow then exhibits a horseshoe-type pattern (Wiggins, 1990). Because of this, trajectories starting from near-by points within an attractor, say $\mathbf{A}_1$, may get separated exponentially as the system evolves. This condition is known as the *sensitive dependence on initial condition*, and the attractor $\mathbf{A}_1$ is then called a *strange attractor.*

A flow f, for a particular initial condition, is said to be chaotic if the trajectories in an attractor exhibit:

1. sensitive dependence on initial conditions but are bounded,
2. irregular and aperiodic behavior, and
3. continuous broad band spectrum.

If $\mathbf{M}$'s Euclidean dimension $d \leq 3$, then graphical techniques can be used to study strange attractors and understand system characteristics. A commonly used method is to plot the continuous system trajectories from a set of initial conditions. The resulting plot is called a *phase portrait.* When $d \geq 3$, the system trajectories can be stroboscopically sampled and plotted corresponding to the state variables of reduced dimension. This plot is called a *Poincaré section plot.*

Graphical analysis based on Poincaré section plots can only provide qualitative understanding of the system dynamics. Quantitative system characterization may be performed using analytical techniques—based on extracting the metric and topological properties of fractal attractors—comprised by *fractal analysis.* The details of fractal analysis are described in the following section.

3 FRACTAL ANALYSIS

The exact dynamics of most realistic systems is not commonly known. Therefore, only the information contained in sensor signals should be utilized to identify the system and reconstruct its dynamics (Casdagli, 1989). This complex task involves the use of many analytical techniques. A plethora of analytical techniques bundled together to make inferences about a particular dynamic system from measured TSD constitute *fractal analysis* for our purposes. Here, *fractal* refers to a mathematical entity having no characteristic length scale, and hence is said to be scale-invariant. Scale-invariance or self-similarity is

[1] A closed and bounded set is said to be compact.

[2] This notation means that every element of $\mathbf{T}$ gets mapped onto another element of $\mathbf{T}$.

[3] Volume elements refer to the small finite chunks of state space.

[4] The concept of dissipative systems emerges from an Eulerian perspective rather than from a Lagrangian one.

commonly encountered in *critical phenomena* (occurring during phase transitions) as well as in systems held far from equilibrium (Arnedo et al., 1992).

In essence, fractal analysis involves 'inverting' the TSD to deduce system characteristics through nonlinear model building. The main objectives of fractal analysis can be broadly categorized depending on the end-purpose as follows:

1. identification of chaos from the system response,
2. establishing the invariants of the system dynamics—for system identification or indirect state estimation, and
3. chaos modeling—when the end-purpose is to capture and later reproduce the system dynamics.

Our interest in this paper lies only in the first two objectives.

3.1 Identification of chaos

The twin assumptions that the dynamics of the given system (in our context, turning dynamics) is chaotic and the sensor signals are not highly contaminated[5] underlie the application of fractal analysis for our purposes. If these assumptions are not valid, the values of metric invariants calculated using fractal analysis have little relevance to the characteristics of sensor signals. An experimental validation of the assumption of the dynamics as being chaotic is therefore essential to the application of fractal analysis. This establishment of dynamics as being chaotic may be done using a battery of tests involving statistical and nonlinear dynamics principles.

In our previous work (Bukkapatnam et al., 1995), we established from experiments that turning dynamics exhibits low dimensional chaos. First, we examined several measured TSD, and the variations of correlation and mutual information functions, thus obtaining Poincaré section plots and lag plots. These plots revealed a definite structure of an attractor. Next, two statistical confirmation tests—the surrogate data test and a novel quasiperiodicity test—and the Lyapunov exponents test were performed.

3.1.1 Surrogate data test

The finite dimensionality of chaotic processes was exploited in this test to confirm the nonlinearity of the system dynamics from several measured TSD. The testing procedure involves three steps: (i) generating many random time-sequences with the same average power spectral density (PSD) as a particular TSD; (ii) constructing a nonlinear predictor model[6] from the surrogate data using lag-coordinates; and (iii) comparing the prediction errors of the surrogate-data-based models with the particular TSD using a non-parametric hypothesis testing procedure. If the prediction errors of the surrogate data-sets are considerably larger than those of the particular measured TSD, then the measured TSD is nonlinear and possibly chaotic.

Non-parametric tests—the Kolmogorov-Smironov test and a z-test based on Mann-Whitney rank-sum statistic (Kennel and Isabelle, 1992)—were employed for hypothesis testing. The prediction errors of all TSD examined were considerably lower than those for the corresponding surrogate data-sets, thus establishing the fact that turning dynamics is indeed nonlinear and possibly chaotic.[7]

3.1.2 Quasiperiodicity test

This test relies on the *representability* of quasiperiodic and chaotic TSD. A quasiperiodic TSD may be represented as a sum of a set of finite periodic sequences. If a given TSD is chaotic, a periodic representation will not be sufficient. Based on this idea, the testing procedure involves representing the given TSD as a sum of finite periodic sequences, and comparing the resulting errors against those obtained by fitting a neural network-based predictor for the same TSD. If the difference in the prediction errors are statistically significant, then the given TSD is not quasiperiodic and very likely to be chaotic.

[5] Contamination refers to both measurement noise and undesirable dynamic contamination.

[6] A local linear predictor model may be adequate for many instances.

[7] We used force and vibration sensor data for our tests. Acoustic emission data was not used because it was not considered reliable.

The application of this test statistically confirmed that the measured TSD, hence turning dynamics, are chaotic.

3.1.3 Lyapunov exponents test

Finally, the Lyapunov exponents test was performed to establish the presence of low-dimensional chaos in turning dynamics. Lyapunov exponents are the best quantifiers of chaos in a dynamical system. They signify the divergence rate, along a particular direction, of small perturbations to an orbit. A system represented by a d dimensional state vector is dissipative if the sum of the d Lyapunov exponents is less than zero and is chaotic when at least one of the Lyapunov exponents is positive. The presence of positive Lyapunov exponents is considered as a reliable confirmatory test for the presence of chaos (Abarbanel et al., 1993).

Since the state vector $\mathbf{x}$ is not readily available, we used several measured TSD for the test. First a particular combination of TSD was used to form a d_E dimensional vector TSD, where d_E is called the embedding dimension. Since the TSD is contaminated by noise, the dominant Lyapunov exponent computed for the TSD will be higher than its actual value. Therefore, the TSD has to be separated from noise. This de-noising was performed using wavelet transforms. The dominant Lyapunov exponents of all TSD were found to be < 2.0 over a range of embedding dimensions $1 \leq d_E \leq 5$; in particular, they hovered between 1.89 and 2.00 when $d_E = 4$, the optimal embedding dimension. It followed therefrom that turning dynamics exhibits low-dimensional chaos. Having established the low-dimensionality of the attractor of the dynamical system corresponding to several measured TSD and hence turning dynamics, we proceeded to extract the system invariants.

3.2 Extraction of system invariants

In order to characterize turning dynamics, the system represented by the sensor signals can be identified by several invariants. These system invariants are evaluated at different instants in time to act as the signal features for estimating the driver.

The invariants in a nonlinear system may be classified into two categories—metric and topological invariants. Metric invariants are the parameters like the various fractal dimensions and Lyapunov exponents that quantify the system dynamics. Topological invariants are integer or rational values that express the relationship (linkage) between simple periodic orbits and the twisting of trajectories near an unstable periodic orbit. Metric invariants and topological invariants together provide a reliable set of invariants for system identification, classification and state estimation. In this work, we use metric invariants, called *fractal dimensions*, described in the following section.

4 FRACTAL DIMENSIONS

The most widely used metric invariants are the fractal dimensions which quantify self-similarity or scale-invariance in the state-space (Takayasu, 1990). Fractal dimensions are measures of the space-filling ability of a solution trajectory in a given attractor. They also yield the number of active degrees of freedom (equivalently, the dimension of the state-space, and hence the *order* of the system) in the underlying dynamical system by virtue of Taken's embedding theorem (Tsonis, 1992).

Fractal dimensions are computed nowadays from a multifractal viewpoint that involves the definition of generalized fractal dimensions D_q, where $q \in [0, \infty)$ is a labeling index. These generalized fractal dimensions constitute a fractal dimension spectrum that has been found useful in extracting the scaling properties of fractals (Arnedo et al., 1992).

Mathematically, a fractal dimension D reveals the proportional relationship between a bulk measure V (such as mass) and a characteristic length measure L of a fractal as per

$$V \propto L^D. \tag{6}$$

More generally, let us consider a fractal $\Gamma \subseteq \tilde{\mathbf{M}}$ where $\tilde{\mathbf{M}}$ is a vector space, and let $\tilde{\mathbf{x}} \in \tilde{\mathbf{M}}$ denote a

point therein.[8] Let there be a density function $\rho(\tilde{\mathbf{x}})$ defined over $\tilde{\mathbf{M}}$. Consider then the bulk function defined in terms of a density function $\rho(\tilde{\mathbf{x}})$ as the integral

$$\mu(\tilde{\mathbf{x}}) = \int_{B_\epsilon(\tilde{\mathbf{x}})} \rho(\tilde{\mathbf{x}}')d\tilde{\mathbf{x}}'. \tag{7}$$

Here, $B_\epsilon(\tilde{\mathbf{x}})$ is an open ball of size ϵ about an arbitrary point $\tilde{\mathbf{x}}$, and $\tilde{\mathbf{x}}'$ is a dummy variable. Then, the pointwise fractal dimension $\alpha(\tilde{\mathbf{x}})$ is given by

$$\alpha(\tilde{\mathbf{x}}) = \lim_{\epsilon \to 0} \frac{d\mu(\tilde{\mathbf{x}})}{d\epsilon}. \tag{8}$$

Usually, $\alpha(\tilde{\mathbf{x}})$ has to be averaged in some sense over $\Gamma \subseteq \tilde{\mathbf{M}}$ to obtain a global fractal dimension.

If we construct a discrete lattice of points $\tilde{\mathbf{x}}_1, \tilde{\mathbf{x}}_2, \ldots$, to cover the fractal Γ upto resolution ϵ, then the global generalized fractal dimension of Γ is given by

$$D_q = \lim_{\epsilon \to 0} \frac{1}{q-1} \frac{log(\sum_j \rho^q(\tilde{\mathbf{x}}_j))}{log(\epsilon)}. \tag{9}$$

The spectrum of fractal dimensions is derived from (9) by substituting different values of $q \in [0, \infty)$. In particular, D_0 corresponds to the capacity (box-counting) dimension, D_1 to information dimension, and D_2 to correlation dimension (Takayasu, 1990). As each of these quantities has been successfully used as a system invariant in diverse applications, we suppose that D_0, D_1 and D_2 will reasonably identify turning dynamics. This is justified because D_0 characterizes the geometry of the attractors, D_1 characterizes the time spent by a solution trajectory in different attractors, and D_2 characterizes the spatial distribution of attractors (Isham, 1993).

5 FRACTAL DIMENSIONS AND TOOL WEAR

We have thus far established that turning dynamics is chaotic and have provided a brief rigorous description of the analytical techniques employed in our paradigm, including the fractal dimensions. Furthermore, we have also described fractal dimensions as system invariants for characterizing turning dynamics.

However, in order to provide a clear motivation for our work, we need to show that fractal dimensions of the measured TSD adequately characterize the variations in turning dynamics and, specifically, that they are sensitive to tool wear. Therefore, first we show from the literature that fractal dimensions of any surface-topography are sensitive to wear. Next, we argue that—since the flank wear land topography affects the measured TSD—the extent and the variation of the flank wear (alternately, flank wear dynamics) will be captured by the fractal dimensions of the sensor signals.

Fractal properties of machined surfaces have been found to be sensitive to tool wear (Zhou et al., 1995). In particular, the fractal dimensions of the machined surfaces have been found to depend on both bearing area and surface roughness. Typical variation of capacity dimension of a shoe surface, when steel roller was moving on the shoe, is shown in Figure 3. The plot is adapted from Zhou et al., (1995). From this figure, it is evident that a definite relationship exists between the capacity dimension of a surface and the extent of wear thereon. Based on this observation, relationships connecting fractal dimensions of the tool wear land and the extent of tool wear may be captured in a fractal-geometry-based wear prediction model, derived from combining the fractal model of contact between rough surfaces (Majumdar and Bhushan, 1991) and the adhesive wear theory.

In the turning process, as the tool wear progresses the physical mechanisms involved therein (such as the formation of multiple cutting edges) modify turning dynamics. This variation of turning dynamics, in turn, alters the force and the vibration patterns associated with the turning process. Hence, the variation of fractal dimensions of the worn surfaces should, in some manner, alter the fractal properties of force and the vibration sensor signals. This is evident from the Artificial Insymmetrized Patterns

[8] For instance, $\tilde{\mathbf{M}}$ may correspond to the state space $\mathbf{M}$ and $\tilde{\mathbf{x}}$ to a realization $\mathbf{x}(t)$ during the evolution of the state vector $\mathbf{x}$ within the attractor, which is represented by Γ.

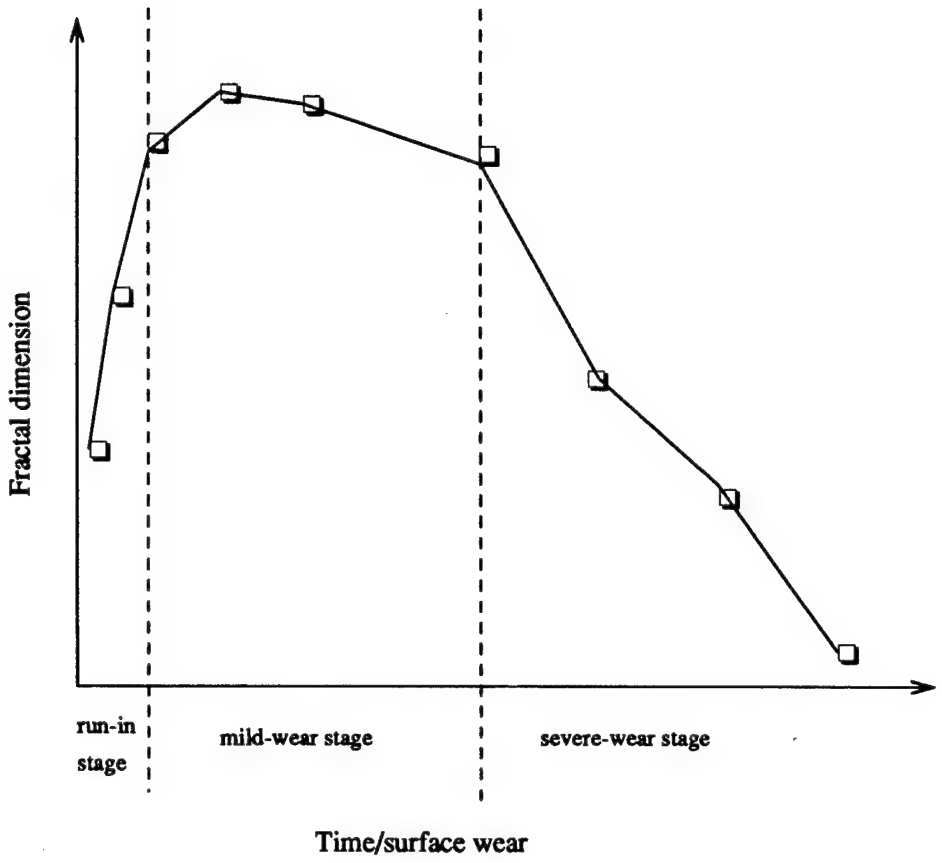

Figure 3: Typical variation of fractal dimension with the surface wear (adapted from Zhou et al. (1995))

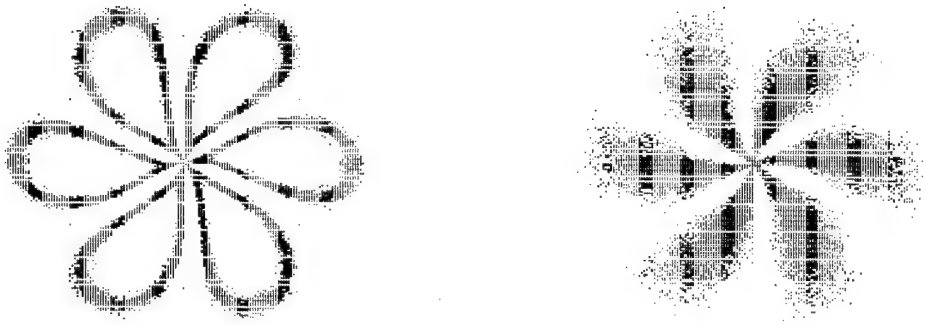

(a) (b)

Figure 4: AIP pattern of main vibration sensor signals—collected at speed = 160 feet/min and feed = 0.0136 inch/rev—capturing the variations in the sensor signals with wear during turning: (a) corresponds to no tool wear ($h_w = 0.0000$ inch) and (b) corresponds to complete tool wear ($h_w = 0.01830$ inch)

(AIPs) (Handley et al., 1993) shown in Figure 4. AIPs were plotted for vibration sensor data collected at a speed of 160 feet/min and feed of 0.0136 inch/rev. AIP zoomed in on the variations in the density distribution with respect to the tool wear. In contrast, Poincaré section plots showed little variation with tool wear (Bukkapatnam et al., 1995).

To summarize the foregoing, the overall interaction may be classified into (i) the effects of tool wear—in particular the fractal properties thereof—on turning dynamics and (ii) the effect of the resulting variations of turning dynamics on the force and vibration sensor signals.

The cutting tool flank wear has the following influences on turning dynamics: It changes (i) tool-workpiece contact characteristics, which in turn affect contact friction; (ii) the shear angle, which directly varies the material removal dynamics; and (iii) cutting edge characteristics due to the formation of multiple cutting edges, which can drastically affect the patterns underlying the force and sensor signals. All these variations alter the thermomechanics of the cutting process.

As a result, the amplitudes and the dominant frequencies of the forces along different component directions vary. Furthermore, the tool wear dynamics may introduce a force component, which is dependent upon the higher spatio-temporal derivatives of the flank wear. The interactions between the cutting force and the machine tool structure result in a variation of the cutting tool vibrations. Thus, the fractal characteristics of the force and the vibration sensor signals possess information sensitive to the tool wear and its higher order derivatives.

6 RESEARCH METHODOLOGY

The objective of our effort is to demonstrate the performance of the generalized fractal dimensions as the signal features for NN-based tool wear estimation in turning. As mentioned in section 1, the methodology consists of

1. performing experiments and obtaining the measured TSD,
2. filtering signal contaminations using wavelet transforms,
3. computation of fractal dimensions, thereby arriving at features to represent a given TSD, and
4. training a recurrent neural network with the extracted features. This trained neural network, when fed with the features extracted from fractal dimensions of filtered TSD, outputs tool wear estimates.

In this overall schema, the procedures of signal separation and feature extraction are crucial, and involve certain theoretical issues. Hence a detailed description of these two procedures is provided in

the following two sections. Since the design of recurrent neural network is more of an implementation issue, description of neural network design is provided in Part-2 of this paper.

7 SIGNAL SEPARATION

Any TSD obtained from the on-line sensors is laden with noise, which has to be properly filtered out. If the TSD were linear, Fourier analysis would have been adequate. But a nonlinear measured TSD can be contaminated by measurement noise and/or dynamical noise (extraneous dynamics). Therefore, separation of contamination from the measured signal becomes very difficult (Schouten et al., 1994).

We used the wavelet transform for signal separation. Our signal separation methodology employed the wavelet representation of a given signal and a soft-threshold function defined from the ***abstract de-noising model*** (Donoho, 1992).

Wavelets are functions whose translations and dilations can be used to represent measurable square-integrable functions. These functions have good time and frequency domain localizations. Let $\mathcal{F}(t) \in L_2^d(\mathbf{R})$, the space of d-dimensional square integrable functions defined over the real line $\mathbf{R}$. Then,

$$\mathcal{F}(t) = \sum_{\mathsf{k}=-\infty}^{\infty} a_{0,\mathsf{k}}\phi_{0,\mathsf{k}}(t) + \sum_{\mathsf{j}=0}^{\infty}\sum_{\mathsf{k}=-\infty}^{\infty} b_{\mathsf{j},\mathsf{k}}\psi_{\mathsf{j},\mathsf{k}}(t), \tag{10}$$

where, $\phi_{\mathsf{j},\mathsf{k}}$ and $\psi_{\mathsf{j},\mathsf{k}}$ are called the scaling and the wavelet functions, respectively; j is the dyadic scale index and determines the central frequency and the frequency range, whereas k is the translation index and determines the time-domain resolution. At a particular scale j, $\{2^{\mathsf{j}/2}\phi(2^{\mathsf{j}}t-\mathsf{k})\}$ and $\{2^{\mathsf{j}/2}\psi(2^{\mathsf{j}}t-\mathsf{k})\}$, $-\infty < \mathsf{k} < \infty$ separately form orthonormal bases in the space of square integrable functions $L_2(\mathbf{R})$. The d-dimensional coefficient vectors $a_{0,\mathsf{k}}$ and $b_{\mathsf{j},\mathsf{k}}$ are obtained from the projection operations

$$\begin{aligned} a_{0,\mathsf{k}} &= <\mathcal{F}, \phi_{0,\mathsf{k}}> = \textstyle\int_{-\infty}^{\infty} \mathcal{F}(t)\phi_{0,\mathsf{k}}(t)dt, \\ b_{\mathsf{j},\mathsf{k}} &= <\mathcal{F}, \psi_{\mathsf{j},\mathsf{k}}> = \textstyle\int_{-\infty}^{\infty} \mathcal{F}(t)\psi_{\mathsf{j},\mathsf{k}}(t)dt. \end{aligned} \tag{11}$$

Thus, a given function $\mathcal{F}(t)$ may be resolved in time-frequency domain as shown in Figure 5. The figure shows that for a particular frequency window (bin), the time-windows are of same width, and the number of time-windows are proportional to the center frequency of a particular frequency window. Furthermore, we see that the width of frequency windows increases logarithmically.

As for a finite length TSD, an empirical wavelet representation of the form

$$\mathbf{\Phi}(n) = \mathcal{S}(\mathcal{F}(t_n)) \tag{12}$$

may be obtained from

$$\mathcal{F}(t) = a_{0,\mathsf{k}}\phi_{0,\mathsf{k}}(t) + \sum_{\mathsf{j}=0}^{\mathsf{J}}\sum_{\mathsf{k}=0}^{2^{\mathsf{j}-1}} b_{\mathsf{j},\mathsf{k}}\psi_{\mathsf{j},\mathsf{k}}(t). \tag{13}$$

Here, $\mathcal{S}(\cdot)$ represents the sampling operation such that the maximum resolution levels correspond to an orthogonally projected subspace $\mathcal{V}_{\mathsf{J}} \in L_2^d(\mathbf{R})$ of scale index $\mathsf{j} = \mathsf{J}$.

However, in general, all measured TSDs $\mathbf{y}(n)$ are contaminated and hence are equivalently stochastic. In such cases, (10) holds with probability 1, as long as the given $\mathbf{y}(n)$ is a ***finite energy sequence*** (Goldberg, 1993). Furthermore, the coefficients $a_{0,\mathsf{k}}$ and $b_{\mathsf{j},\mathsf{k}}$ correspond to the transform vector codebooks.

But, in our case, we need to project $\mathbf{y}$ into the space of the unknown function $\mathbf{\Phi}$. This relationship in the wavelet domain[9] may be expressed as follows:

$$\mathcal{W}^{\mathsf{j},\mathsf{k}}\mathbf{y} = \mathcal{W}^{\mathsf{j},\mathsf{k}}\mathbf{\Phi} + E_e^{\mathsf{j},\mathsf{k}}v, \tag{14}$$

[9]Wavelet domain refers to the space of the wavelet coefficients.

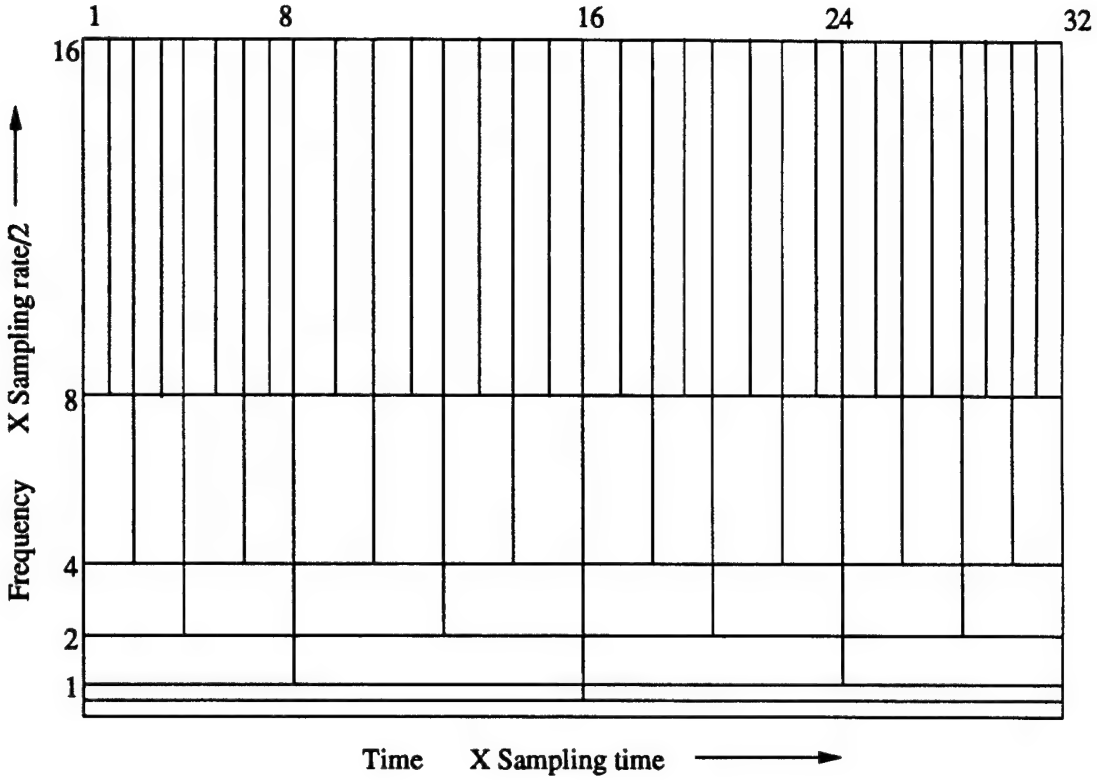

Figure 5: Resolution of a given function in time-frequency domain by wavelet transform

where $\mathcal{W}^{j,k}(\cdot)$ denotes a vector corresponding to a particular coefficient of wavelet transform of $\mathbf{y}$, v is an independent and identically distributed standard Gaussian vector and $E_e^{j,k}$ is a diagonal matrix whose diagonal elements e_j's correspond to the ***noise levels*** (Donoho, 1992). This relationship holds reasonably well for many measured TSD as long as the desired signal is low-dimensional compared with any contaminant, and the TSD is reasonably long. In such cases, for each component y_j of $\mathbf{y}$,[10], and for every scale j a soft threshold

$$\tau_j^j = e_j^j \sqrt{log_2 N} \tag{15}$$

may be computed, and then applied on every wavelet transform coefficient thereof so that the resulting thresholded coefficients may be expressed as

$$\mathcal{W}^{j,k}\tilde{y_j} = sgn(\mathcal{W}^{j,k}y_j)(|\mathcal{W}^{j,k}y_j| - \tau_j^j),\ 1 \leq j \leq d_{\mathbf{y}}, \tag{16}$$

where $sgn(\cdot)$ denotes the signum function. In (14), (15) and (16) the only unknown independent quantities are e_j^j. Based on (Johnstone and Silverman, 1995), we may approximate e_j^j to be the standard deviation of the coefficients at scale j. This is a valid approximation because (i) the measured TSD is reasonably stationary, (ii) the covariance matrix reveals a reasonable short-term periodicity (as is evident from the Poincaré section plots drawn in (Bukkapatnam et al., 1995)). These conditions incidentally are the requirements for the approximation to hold. This soft thresholding procedure is applied to every $y_j(n)$ to carry out signal separation, and the filtered signal used for feature extraction.

[10]Note that the measurement vector $\mathbf{y}$ is a vector TSD, whose components—i.e, y_j's—are scalar TSD.

8 FEATURE EXTRACTION

The filtered signal is still uncompressed and the size of the TSD file much too large. Such huge uncompressed data is unwieldy for training a neural network. So, as proposed earlier, the generalized fractal dimensions (D_0, D_1, and D_2) may be used as signal features. Our procedure for estimating the fractal dimensions is based on the algorithm developed by Liebovitch and Toth (1989). The procedure for computing the fractal dimensions is as follows:

For a given vector TSD, the data points corresponding to each scalar TSD are scaled to lie between 0 and 1. Then, the data points are shifted and rescaled to lie between 0 and a large value 2^m, typically $m = 32$ will be sufficient. Precisely m values of ϵ are chosen. For each chosen value of ϵ,

1. the number of balls $\mathsf{N}(\epsilon)$ required to cover the fractal drawn in the space of the given vector TSD, and
2. the frequency $p_i(\epsilon)$ of points in each of these balls

are determined, from which bulk V can be obtained (Tsonis, 1992). The generalized dimensions may be deduced from the slope of the linear portion of log V_q versus log ϵ graph, representatives of which are shown in Figure 9 of Part-2 of this paper.

However, the fractal dimensions thus obtained are sensitive to the dimension d_E of the vector TSD, which is synonymous with the embedding dimension. The exact fractal dimensions in such situations can be found by stabilizing their value with increasing embedding dimension. This can be achieved either by including an additional lag coordinate, or an independent TSD (Tsonis, 1992). In our work, we increased the dimension of the vector TSD by including the data from several sensors till the values of fractal dimensions stabilized.

One important issue here is that if we do not have enough number of points (i.e., the vector TSD is not sufficiently long), there is a possibility of ***wandering intercepts*** (Cutler, 1991) which will render the estimates of fractal dimensions inaccurate. However, the more the number of points, the larger is the computational effort for calculating $p_i(\epsilon)$. We deem the latter criterion of computational speed as the more important one, because our results showed (see Part-2 of this paper) that the $p_i(\epsilon)$ versus ϵ plot was reasonably linear over ≥ 3 decades. Thus, we were justified in using Liebovitch and Toth algorithm.

Fractal dimensions computed thus may be used as features from which exemplar patterns to train a recurrent neural network may be prepared. The neural network trained using these exemplar patterns functions as a fractal estimator. Our implementation details and results are presented in the next part of the paper.

9 SUMMARY

This paper addressed most of the theoretical issues, that led to the development of a generalized methodology of fractal estimation of flank wear in the turning process. The major contributions of this paper are the development of novel paradigms for signal separation and feature extraction. The implementation issues are addressed in Part-2 of this paper.

Acknowledgments

The authors wish to thank the National Science Foundation for their support for this research under grants NSF-DDM 9223181 and NSF-DDM 9301690. In addition Dr. Soundar R. T. Kumara wishes to acknowledge the Army Research Office for their support under the grant DAA H04-96-1-0082.

References

Abarbanel, H., Brown, R., and Tsimiring, L., 1993, "The analysis of observed chaotic data in physical systems," *Reviews of Modern Physics*, Vol. 65, pp. 1331–1422.

Arnedo, A., Argoul, F., Muzy, J., Pouligny, B., and Freysz, E., 1992, "The optical wavelet transform," In *Wavelets and their Applications*: Ruskai et al. (eds), Jones and Bartlett, New York.

Boothroyd, G., and Knight, W. A., 1989, Fundamentals of Machining and Machine Tools, Marcel Dekker, New York.

Bukkapatnam, S. T. S., Lakhtakia, A., and Kumara, S. R. T., 1995, "Analysis of sensor signals shows that turning process on a lathe exhibits low-dimensional chaos," *Physical Review E*, Vol. 52, pp. 2375–2387.

Casdagli, M., 1989, "Nonlinear prediciton of chaotic time-series," *Physica D*, Vol. 35, pp. 335–356.

Cutler, C., 1991, "Some results on the behavior and estimation of fractal dimensions of distributions on attractors," *Journal of Statistical Physics*, Vol. 62, pp. 651–708.

Donoho, D., 1992, "De-noising by soft-thresholding," Technical Report: Department of Statistics, Stanford University, Stanford, CA.

Elanayar, S., and Shin, Y. C., 1995, "Robust tool wear estimation with radial basis function neural networks," *ASME Journal of Dynamic Systems, Measurements and Control*, Vol. 117, pp. 459–467.

Du, R., Elbestawi, M. A., and Wu, S. M., 1995, "Automated monitoring of manufacturing processes, Part 1: Monitoring methods," *ASME Journal of Engineering for Industry*, Vol. 117, pp. 121–132.

Goldberg, A., 1993, "Applications of wavelets to quantization and random process representations," Ph. D. Thesis, Department of Electrical Engineering, Stanford University, Stanford, CA.

Handley, J. W., Janisch, H. M., Bjork, C. A., Richardson, L. T., and Carruth, R. T., 1993, "Chaos and fractal algorithms applied to signal processing and analysis," *Simulation*, Vol. 60, pp. 261–279.

Hardt, D. E., 1993, "Modeling and control of manufacturing processes: Getting more involved," *ASME Journal of Dynamic Systems Measurement and Control*, Vol. 115, pp. 291–300.

Isham, V., 1993, "Statistical aspects of chaos: A review," In *Networks and Chaos—Statistical and Probabilistic Aspects*: Barndorff-Nielsen et al. (eds), Chapman and Hall, London, UK.

Johnstone I. M., and Silverman, B. W., 1995, "Wavelet threshold estimators for data with correlated noise," Technical Report No. 469: Department of Statistics Stanford University Stanford, CA.

Kamarthi, S. V., 1994, "On-line flank wear estimation in turning using multi-sensor fusion and neural networks," PhD Thesis, Department of Industrial and Manufacturing Engineering, University Park, PA.

Kennel, M., and Isabelle, S., 1992, "Method to distinguish possible chaos from colored noise and determine embedding parameters," *Physical Review A*, Vol. 46, pp. 3111–3114.

Kumara, S. R. T., Kamarthi, S. V., Bukkapatnam, S. T. S., and Lee, J. W., 1994, "Sensor based monitoring for real-time quality control in manufacturing," *Proceedings of AAAI-94 Spring Symposium*, Stanford, CA.

Liebovitch, L., and Toth, T., 1989, "A fast algorithm to determine dimensions by box counting," *Physics Letters A*, Vol. 141, pp. 386–390.

Majumdar, A., and Bhushan, B., 1991, "Fractal model of elastic-plastic contact between rough surfaces," *ASME Journal of Tribology*, Vol. 113, pp. 1–11.

Schouten, J. C., Takens, F., and Van Den Bleck, C. M., 1994, "Estimation of the dimension of a noisy attractor," *Physical Review E*, Vol. 50, pp. 1851–1861.

Stark, H., and Wood, J., 1994, Probability Random Processes and Estimation Theory, Prentice-Hall, Englewood Cliffs, NJ.

Takayasu, H., 1990, Fractals in Physical Sciences, Manchester University Press, London, UK.

Trent, E.M., 1991, Metal Cutting. Butterworth, Oxford, UK.

Tsonis, A., 1992, Chaos – From Theory to Applications. Pergamon Press, NY.

Ulsoy, A. G., and Koren, Y., 1993, "Control of machining process," *ASME Journal of Dynamic Systems Measurement and Control*, Vol. 115, pp. 301–308.

Wiggins, A., 1990, Introduction to Applied Nonlinear Dynamical Systems and Chaos. Springer–Verlag, NY.

Zhou, G., Leu, M., and Blackmore, D., 1995, "Fractal geometry modeling with applications in surface characterization and wear prediction," *Internation Journal of Machine Tool and Manufacturing*, Vol. 35, pp. 203–209.

List of symbols

$\mathbf{A}$	:	Attracting set
$\mathbf{A}_j$	:	Attractor, $j = 1, 2, ...$
a, b	:	Wavelet transform coefficients
$B_\epsilon(\mathbf{x})$	:	Open ball of size ϵ about $\mathbf{x}$
D	:	Fractal dimension
D_q	:	Generalized fractal dimensions $q \in [0, \infty)$
d	:	Dimension of $\mathcal{F}$ defined in Section 7
d_E	:	Embedding dimension
$d_{\mathbf{p}}$	:	Process parameter vector dimension
$d_{\mathbf{x}}$	:	State space dimension
$d_{\mathbf{y}}$	:	Measurement space dimension
$E_e^{\mathsf{j},\mathsf{k}}$	:	Noise level matrix
e_j	:	Noise level for j^{th} TSD
$F(\cdot)$	:	Vector field defined in Section 2
$\mathcal{F}(t)$	:	A function defined in $L_2(\mathbf{R})$
$f(\cdot)$	:	Flow operator defined in Section 2
$\mathbf{G}$	:	Performance space
J	:	Maximum resolution
j	:	Dummy time index
j	:	Dilation (dyadic scale) index
K	:	Number of state variables of interest
k	:	Translation index
L	:	Length measure
$\mathbf{M}$	:	State space
$\tilde{\mathbf{M}}$	:	An arbitrary space containing the fractal Γ
m	:	Binary power index defined in Section 8
N	:	Length of TSD
N	:	Number of ball (boxes) to cover a given fractal
n	:	Time index
P	:	A point on tool surface
$\mathbf{P}$	:	Process parameter vector
p	:	Component of $\mathbf{p}$
q	:	Index of generalized fractal dimensions
$\mathbf{R}$	:	Real line
$\mathcal{S}$	:	Sampling operation transformation
s	:	Abstract process state
$sgn(\cdot)$	:	Sign function
$\mathbf{T}$	:	A compact set defined in Section 2
t	:	Time variable
t_1	:	Time interval between successive tool wear estimates
t_2	:	Sampling time of the measured TSD
t_w	:	Moving time window for thresholds and fractal dimensions
$\mathbf{U}$	:	Space of state variables
$\{u\}$	:	State variable
V	:	Bulk measure
$\mathcal{V}_J$	:	Vector space of $L_2(\mathbf{R})$ corresponding to resolution J
v	:	Independent and identically distributed random variable
$\mathcal{W}^{\mathsf{j},\mathsf{k}}(\cdot)$	:	Wavelet transform
$\mathbf{w}$	:	Tool wear (state) vector
$\mathbf{x}$	:	State vector
$\tilde{\mathbf{x}}$	:	A vector lying in $\tilde{\mathbf{M}}$ space

$\mathbf{x}_D$	:	Driver vector
$\mathbf{x}_R$	:	Response vector
x	:	Component of state vector
$\mathbf{Y}$	:	Measurement space
$\mathbf{y}$	:	Measurement vector
y	:	Measurement variable
$\mathbf{Z}$	:	Space of integers
z	:	Performance variable
$\alpha(\cdot)$	:	Pointwise fractal dimension
Γ	:	Fractal
ϵ	:	Size of an open ball
$\mu(\cdot)$	:	Bulk parameter
$\mho$	:	Basin of attraction
Ω	:	Sample space of s
$\mathbf{\Phi}$	:	Unknown function onto which $\mathbf{y}(k)$ is projected
$\phi(t)$	:	Scaling function
$\psi(t)$	:	Wavelet function
$\rho(\cdot)$	:	Density function
ϑ	:	Measurement contamination
ϖ	:	Dynamic contamination
τ	:	Soft threshold
ζ	:	Time-series vector
$\tilde{\zeta}$	:	Denoised vector time-series vector